

A Small Spot, Inert Gas, Ion Milling Process as a Complementary Technique to Focused Ion Beam Specimen Preparation

Paul E. Fischione,^{1,*} Robert E.A. Williams,² Arda Genç,² Hamish L. Fraser,²
Rafal E. Dunin-Borkowski,³ Martina Luysberg,³ Cecile S. Bonifacio,¹ and András Kovács³

¹*E.A. Fischione Instruments Inc., 9003 Corporate Circle, Export, PA 15632, USA*

²*Center for the Accelerated Maturation of Materials, The Ohio State University, 1305 Kinnear Road, Columbus, OH 43212, USA*

³*Ernst Ruska-Centre for Microscopy and Spectroscopy with Electrons and Peter Grünberg Institute, Forschungszentrum Jülich GmbH, Wilhelm-Johnen-Straße, 52425 Jülich, Germany*

Abstract: This paper reports on the substantial improvement of specimen quality by use of a low voltage (0.05 to ~1 keV), small diameter (~1 μm), argon ion beam following initial preparation using conventional broad-beam ion milling or focused ion beam. The specimens show significant reductions in the amorphous layer thickness and implanted artifacts. The targeted ion milling controls the specimen thickness according to the needs of advanced aberration-corrected and/or analytical transmission electron microscopy applications.

Key words: ion milling, focused ion beam, amorphous damage, implantation, artifact

INTRODUCTION

Significant information about a material's chemistry, magnetic properties, atom locations, surface characteristics, and microstructure can be obtained through transmission electron microscopy (TEM), which requires artifact-free specimens to quantify these properties in two and three dimensions.

The TEM specimen preparation techniques used most commonly involve broad-beam Ar ions or focused ion beam (FIB), milling using Ga ions in a scanning electron microscope. Surface damage and unintended ion-implanted layers incurred during the preparation process are some artifacts that limit the information that is obtainable from analytical and high-resolution electron microscopy. Deleterious surface layers are often a significant fraction of the total specimen thickness, which affects both the quality and quantity of the results.

Within the past 20 years, FIB systems incorporating Ga ion beams of up to 50 keV have been applied to preparing specimens for TEM analysis from almost any solid material. The thinning and extraction of TEM specimens with accuracy and site-specificity is an advantage of FIB (Kirk et al., 1989; Young et al., 1990; Basile et al., 1991; Giannuzzi & Stevie, 1999; Anderson & Klepeis, 2005; Kamino et al., 2005; Jia et al., 2014). A significant fraction of the specimens produced at any given laboratory is now prepared using FIB technology.

Advances in aberration-corrected TEM imaging, monochromation, and enhanced analytical methods have been achieved during the past decade (Batson et al., 2002).

Techniques such as energy-dispersive X-ray spectroscopy (EDXS), electron energy-loss spectroscopy (EELS), high-angle annular dark-field (HAADF) detection, and energy-filtered imaging are routinely used for elemental identification and quantification. Electron tomography for three-dimensional imaging has also become a common technique for the physical sciences.

These improvements in the resolution and analytical capabilities of modern microscopes require the minimization of artifacts incurred during the preparation process. For example, artifacts of specimen thinning with a Ga ion beam may include surface amorphization, Ga implantation, and the generation of crystallographic defects (Barna, 1991; Barber, 1993; Barna et al., 1999; McCaffrey et al., 2001; Kato, 2004; Anderson & Klepeis, 2005; Mayer et al., 2007; MoberlyChan et al., 2007; Volkert & Minor, 2007). Similarly, specimens prepared by electrolytic polishing or conventional mechanical grinding followed by broad-beam ion-thinning methods can also exhibit surface damage (Barna, 1991; Barna et al., 1999). Disordered surface layers, such as thin native oxides, have also been shown to contribute significantly to surface plasmon excitations in low-loss EELS (Scheu et al., 2003; Mkhoyan et al., 2007).

Low energy (<1 keV), inert gas ion milling is an attractive method (Barna, 1991; Barber, 1993; Barna et al., 1999; Kato, 2004; Genç et al., 2007; Mayer et al., 2007; MoberlyChan et al., 2007; Volkert & Minor, 2007; Miyajima et al., 2010; Mehrtens et al., 2012; Lotnyk et al., 2015) for lessening the effects of surface damage. For crystalline materials, the ideal procedure is to reduce progressively the specimen thickness by removing surface damage layers while leaving the material beneath undisturbed. Surface damage can constitute a substantial

Received October 3, 2016; accepted April 6, 2017

*Corresponding author. pe_fischione@fischione.com

fraction of the total specimen thickness (Giannuzzi, 2006); therefore, reducing the layer thickness can yield thin specimens that are ideal for a variety of imaging and analytical techniques.

For example, the use of high-resolution transmission electron microscopy (HRTEM) and EELS often require specimens to be thinned to meet weak-phase object criteria and ideally represent the single scattering regime. The preparation challenge is compounded for small ($\sim 10 \times 5 \mu\text{m}$) FIB lift-out specimens because post-FIB damage removal based upon broad-beam ion milling risks redeposition, that is, a broad beam covers not only the area of interest, but also affects other parts of the specimen, such as the support grid onto which the FIB lamella is mounted and the protective cap layer. As a consequence, material from the grid and the cap are sputtered and partly redeposited onto the specimen. Therefore, the ability to focus and selectively target the milling area is highly desirable to avoid unintended sputtering and redeposition.

One of the most important criteria for TEM specimen preparation is to produce an electron-transparent region that is representative of the bulk material's structure and properties while reducing preparation-induced artifacts to a minimum. The primary preparation-induced artifacts generated during ion milling are the following:

Ion implantation: The accelerated Ga ions penetrate the specimen surface creating an artificial layer that has different properties than the bulk material. Such "dead layer" formation is a major problem for studies of semiconductor properties in p - n junctions or magnetic materials (Cooper et al., 2009). Post-FIB, low energy, Ar ion milling is able to remove the Ga-contaminated layer because Ar is lighter than Ga and rarely forms chemical bonds with other elements (Unocic et al., 2010).

Amorphization: For both Ga and Ar ions, the high-energy ionic particles break the chemical bonds of the crystalline materials and create an amorphous layer on the surface. Formation of amorphous layer is materials-dependent; semiconductor and ceramic materials easily amorphize when compared with metals (Huh et al., 2013). Decreasing the energy and the incident angle of the incoming ions can reduce the effect (Barna et al., 1998).

Surface roughness: The sputtering ions create volume defects due to surface inhomogeneities and the resulting sputtering rate differences. Typically, ceramics, oxides, and multi-phase alloy systems are sensitive to milling-induced surface roughness. The degree of surface roughness is exacerbated when specimens contain layers or phases with different sputtering rates, for example, substrate (sputtering rate V_1), layer (V_2), protective layer (V_3), and $V_1 \neq V_2 \neq V_3$. Low angle, low energy, Ar ion milling, combined with either beam rastering or specimen oscillation, can reduce the effect.

Redeposition: Cu, Pt, Au, or other sputtered material from the FIB lamellae support and the protective cap layer can redeposit onto the surface of lamellae. The effect can be fully eliminated by focusing the Ar ion beam at the lamellae and by positioning the lamellae on the support grid in a way that ions

only interact with the area of interest on the lamellae. This method is made possible by the use of Everhart-Thornley detector technology to image ion-induced secondary electrons, which provides an exact representation of the area being milled.

Heating: Sputtering of the surface is a localized thermal effect associated with the energy applied during milling, which can lead to amorphization, intermixing, and selective etching of the materials. Cooling the specimen during ion milling can reduce the effect (Bahnck & Hull, 1990).

The benefits of low energy, inert gas (Ar) ion milling for the removal of amorphous and implanted surface layers, and the improvement of microscopy results are described in this paper.

FIB Lift-Out and Focused Ar Ion Beam Milling

TEM specimen preparations of semiconductor materials systems will be presented that represent characteristic cases for surface amorphization and roughness. An example for beam-sensitive material that required low-voltage TEM and very thin specimen thickness is also presented.

For conventional ion beam technology, the size of the Ar ion beam can vary from $\sim 300 \mu\text{m}$ to 1.5 mm full-width at half-maximum (FWHM). The advantage of broad-beam technology is that ions can be generated at a sufficiently low energy to minimize specimen damage; however, at low energy, the ion beam diameter can greatly increase to a few millimeters. In a FIB, the Ga ion beam diameter can be on the order of 5 nm (Utke et al., 2008). An advantage of FIB is that the use of a liquid metal (Ga) nanometer-sized beam is often combined with an electron column for imaging during the preparation process, which enables site-specific specimen preparation. However, specimen thinning with a Ga ion beam at sufficiently low energy can be a time-consuming process and requires a skilled user and a very stable, well-aligned system (Schaffer et al., 2012).

The challenge was to develop a technology that used inert ions to avoid chemical alteration, low energy to minimize amorphous layers, low temperature to reduce heat-induced damage, and a small ion spot to prevent redeposition. With these criteria, a unique ion source technology was developed: an ion beam of sufficiently low energy (as low as 50 eV), concentrated into a small spot (as small as $1 \mu\text{m}$), that produced sufficient current (~ 100 – 150 pA) to allow for reasonable milling rates (~ 1 – 8 nm/min). Milling rates are dependent upon the accelerating voltage of the incident ions, the corresponding beam current, the milling angle, and the size of the area targeted by the rastered ion beam. To investigate the effect of a small-spot Ar ion beams to produce high-quality electron transparent specimens, TEM and scanning transmission electron microscopy (STEM) specimens of several important materials classes were chosen for this study.

The ion source developed for this application uses electrons from a thermionic emitter (filament) to ionize argon gas. A series of electrodes, biased at voltages relative to the filament, guide the primary electrons into an ionizing chamber. A mass flow controller regulates argon gas flow. Collisions between

electrons and gas atoms produce ions that are primarily positive and singularly charged. Some of the ions escape through an aperture and are accelerated through an electrostatic lens. The result is that ions impact only a small area of the specimen. Varying the bias on the lens changes its focal plane and allows the spot size to be adjusted. The voltage of the ionizing chamber determines the final particle energy at the target (the specimen), which is maintained at ground potential. Electrostatic deflectors, located at the exit of the lens, steer the beam transverse from its main axis in two directions (horizontal and vertical), which allows positioning of the spot relative to the target. Under computer control, the deflectors can scan the beam across a field of view or locate it at arbitrary points.

To establish the position of the ion beam with respect to the specimen, an Everhart–Thornley-type secondary electron detector (SED) was incorporated to image ion-induced secondary electrons. The ion source was fitted to a vacuum chamber possessing a specimen stage that can both rotate the specimen to achieve an appropriate initial orientation and tilt to yield milling angle adjustability. To further reduce the possibility of specimen damage, the stage was thermally attached to a liquid nitrogen dewar that allows ion milling to occur at cryogenic temperatures (approximately $-170\text{ }^{\circ}\text{C}$). The chamber was also equipped with a Faraday cup to monitor ion beam current.

MATERIALS AND METHODS

The materials investigated in this study include semiconductor Si (Figs. 1, 2); MnAs on GaAs (Figs. 3, 4); oxide semiconductor Co:ZnO on Al_2O_3 (Fig. 5); a multilayer of CaTiO_3 and SrTiO_3 (Fig. 6); a $\text{Sr}_2\text{FeMoO}_6$ thin film grown on SrTiO_3 (Fig. 7); a Ni-based superalloy (Fig. 8); and a structural Ti alloy (Figs. 9, 10) (Li & Yang, 2002). The application examples of the benefit of low-energy-focused ion milling presented required different specimen thicknesses in the range of few nanometers to a few tenths of nanometers according to the imaging or spectroscopy characterization methods.

Specimens of Si milled with a Ga ion beam were first prepared to assess the surface chemistry and thickness of damage. To best prepare FIB lift-out specimens for TEM-EDXS analysis, a capping layer of $1\text{--}2\text{ }\mu\text{m}$ of Pt was electron beam deposited to protect the as-milled surfaces from further alteration by the Ga ion beam. HRTEM and STEM imaging and microanalysis were conducted. Specimens for the other TEM analyses in this work were prepared by mechanical polishing and conventional broad-beam Ar ion milling.

The FIB specimens were prepared using a Helios NanoLab 400S dual beam system (Thermo Fisher Scientific, Waltham, MA, USA) equipped with a micromanipulator (Omniprobe, Oxford Instruments NanoAnalysis, High Wycombe, UK) and gas injection system for deposition of Pt/C and pure C protective layer on the surface of the specimen. Post-FIB, low energy ($<1\text{ keV}$) Ar ion milling was conducted using $\sim 1\text{-}\mu\text{m}$ diameter concentrated ion beam in a NanoMill TEM specimen preparation system (E.A. Fischione Instruments, Inc., Export, PA, USA). The steps of the post-FIB ion milling processes and the important parameters are listed in Table 1.

Both conventional and aberration-corrected TEM observations were used to image the ion-milled specimens. In some cases, conventional TEM was preferred as a quality check of the specimens because it is more sensitive to surface inhomogeneities caused by image contrast than the aberration-corrected TEM images that usually do not use an objective aperture for image recording. For TEM studies, the following microscopes were used: a TEAM 0.5 (United States Department of Energy, Lawrence Berkeley National Laboratory, Berkeley, CA, USA) operated at 80 keV, Tecnai G2 and TF20 (Thermo Fisher Scientific) operated at 200 keV, a CM200 (Philips, Koninklijke Philips N.V. Amsterdam, The Netherlands), and an aberration-corrected Titan (Thermo Fisher Scientific) operated at 80 and 300 keV.

The decrease in surface damage was characterized between milling sessions by applying fast Fourier transforms (FFT) on the acquired images, which indicate the periodicities conveyed by the objective lens in phase contrast imaging. The diffuse halo contrast, located near the central region of the FFT, is associated empirically with surface amorphization, such that the number of frequencies present in the FFT increase and the central halo decreases as the amorphous surface layer is reduced. By initially considering a material's sputtering threshold and progressively reducing the Ar ion beam energy, a steady-state operating point is desired—whereby the rate of damage removal outweighs the potential for the creation of new damage (Barnard et al., 2006).

Different dual beam systems may have different parameters and additional steps in TEM specimen preparation. Table 1 summarizes the main procedure and parameters of TEM specimen preparation using FIB and NanoMill system that became a standard procedure at the Ernst Ruska-Centre. Because the NanoMilling process is incorporated into the specimen preparation procedure, low-energy Ga ion milling ($<5\text{ keV}$) in the FIB is omitted.

The thickness of the electron beam-deposited protective layer is typically in a range of $100\text{--}500\text{ nm}$, whereas the ion beam deposited Pt/C layer is $\sim 3\text{-}\mu\text{m}$ thick. Deposition of amorphous carbon and/or the Pt/C layers on the surface of the lamellae can be advantageous in tuning the aberration corrector of the microscope.

RESULTS AND DISCUSSION

Beam Size and Surface

TEM images collected before and after targeted, low-energy Ar ion milling^a demonstrate that the amorphous damage layer has been reduced in thickness, as will be demonstrated in the following.

The removal of thin, damaged surface layers necessitates the use of relatively slow milling rates to avoid over-thinning the lamella, which could result in diminished structural integrity of the specimen. Atomic force microscopy was used

^aThroughout the paper “Ar ion milling” refers to small spot Ar ion milling, if not stated otherwise.

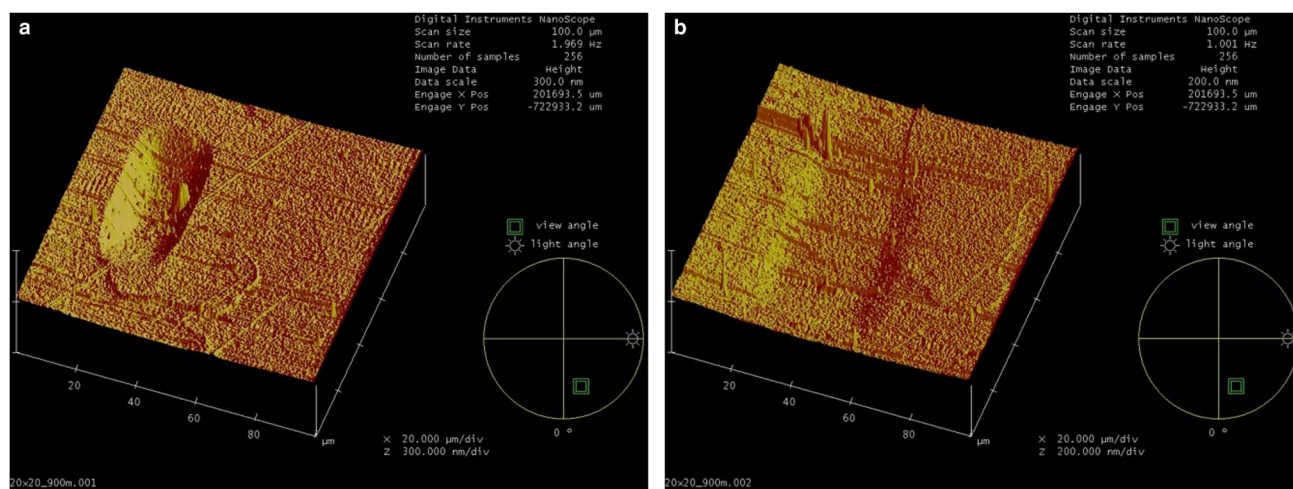


Figure 1. Si specimen topography after targeted 900 V Ar ion milling. **a:** $20 \times 20 \mu\text{m}^2$ area. **b:** $40 \times 40 \mu\text{m}^2$ area. Milling rates were 7.7 and 2.0 nm/min, respectively.

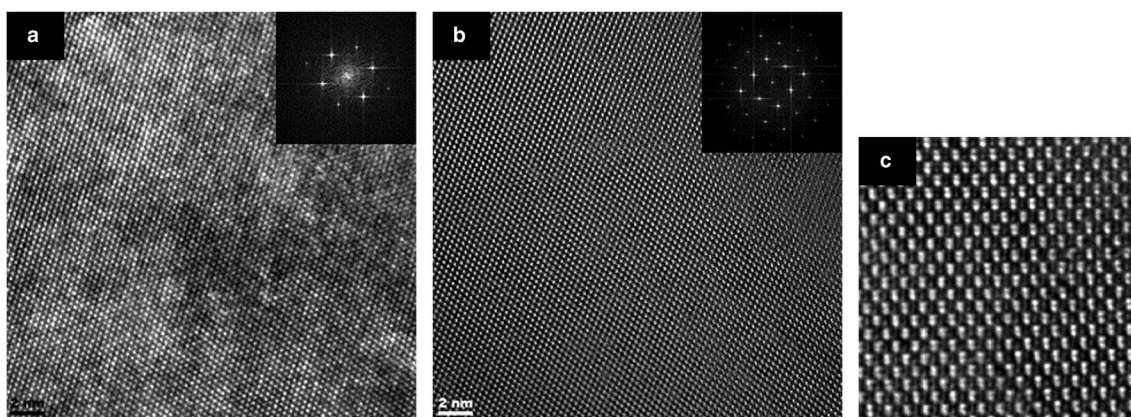


Figure 2. Si specimen before (a) and after (b) milling using a 200 eV Ar ion beam. A final specimen thickness of ~ 7 nm after milling resulted to sub-Ångström lattice spacing evident as shown in image (b) and fast Fourier transform (inset of b). c: Shows the 1.35 Å dumbbell spacing of Si. Images (b) and (c) were acquired using the TEAM 0.5 at an operating voltage of 80 keV.

to measure these rates on Si (100) specimens and to show the shape of the milled areas, as presented in Figure 1. Depending upon the milling area chosen, milling rates for the 900 eV Ar ion beam vary from 7.7 to 2.0 nm/min for raster box sizes of $20 \times 20 \mu\text{m}^2$ and $40 \times 40 \mu\text{m}^2$, respectively.

Silicon

Silicon is the most widely used semiconducting material from which integrated circuits are created. Virtually all commercially available microelectronic devices are Si-based. Pure silicon is not a conductor; therefore, “doping” pure silicon with very small amounts of elements such as boron or phosphorus give it semiconducting properties that are ideal for electronic devices. Because of the ubiquitous nature of silicon in the semiconductor industry, a silicon specimen was prepared for this research. Figure 2 demonstrates that by thinning with a 200 eV Ar ion beam, high-quality TEM specimens can be achieved that allow for imaging with sub-Ångström resolution.

MnAs on GaAs Substrate

MnAs is a room temperature ferromagnetic pnictide that can be easily grown in epitaxy with semiconductor substrates of GaAs and Si (Das et al., 2003). Figure 3a shows a bright-field transmission electron microscopy (BF-TEM) image of the FIB-prepared specimen before low-energy Ar ion milling. Figure 3b displays a HRTEM image of the same location. The dark-contrast variation in GaAs in Figure 3b is due to the presence of a damaged layer on the surface. The specimen was Ar ion milled from both sides at 900 and 500 eV energies and incident angles of 10 and 12°, respectively. The Ar ion milling was precisely targeted on the specimen using the NanoMill system’s SED; the SED image is shown in Figure 3c. Low-energy ion milling successfully removed most of the specimen damage, as shown in Figure 3d.

The high-energy sputtering process with Ga ions not only damages the surface of the specimen, but also makes it rough.

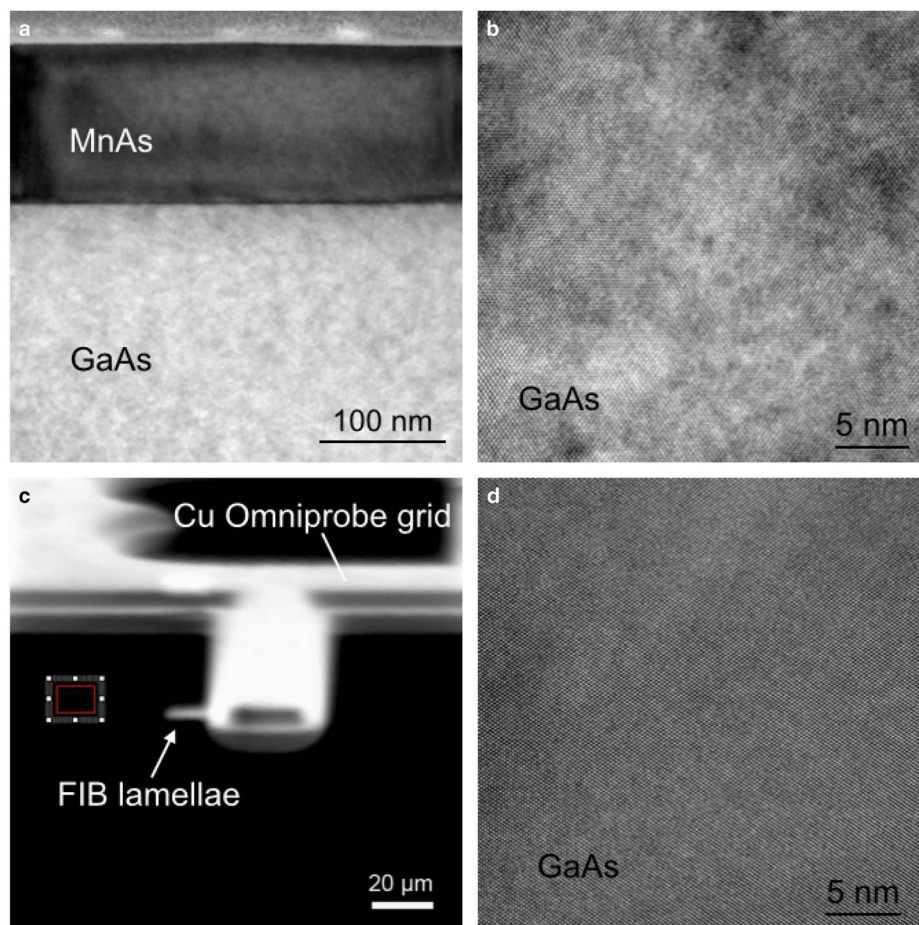


Figure 3. **a:** Bright-field transmission electron microscopy image of MnAs on GaAs after focused ion beam (FIB) preparation finished at 5 keV. **b:** High-resolution transmission electron microscopy (HRTEM) image of GaAs showing the patchy contrast due to surface amorphization and roughness. **c:** Image of the FIB lamella and Omniprobe grid in the NanoMill system. Ion beam energy is 900 eV, tilt 15°. **d:** HRTEM image of GaAs after ion milling at 500 eV at 12° for 30 min.

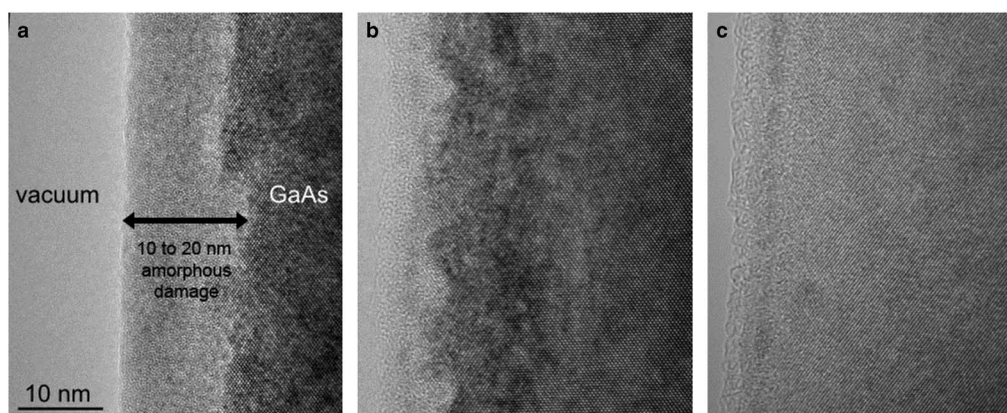


Figure 4. High-resolution transmission electron microscopy images of GaAs edge after (a) focused ion beam preparation at 5 keV, (b) Ar ion milling at 900 eV for 10 min at 10°, and (c) Ar ion milling at 500 eV for 20 min at 10°.

Figure 4 shows the improvement in specimen condition as it moves through the low-energy ion milling process. The 5 keV energy Ga ion beam produced a 10- to 20-nm thick

amorphous layer on GaAs and an inhomogeneous surface with ~5 nm roughness, as shown in Figure 4a, where the roughness can be estimated from the jagged edge of the

crystalline part of the specimen. Ar ion milling at 900 eV for 10 min removed most of the amorphous layer from the surface, but the milling process was not sufficiently long to remove all the FIB damage and the roughness remained relatively the same. Additional milling at 500 eV removed almost all the amorphous GaAs from the surface and roughness was reduced, as well. The removal of the surface damage part of the specimen results in a reduced thickness, which may improve the image contrast of the BF-TEM image.

Co:ZnO on Al₂O₃ Substrate

Oxides are popular as substrates in thin-film growth technologies to generate various epitaxial layers. Oxide materials, in interaction with high-energy ions, typically form a lesser amount of an amorphous layer on the surface, but are more sensitive to selective sputtering, which may result in a high surface roughness. Figure 5 shows the images of Co-doped ZnO thin film (Kovács et al., 2013) deposited on Al₂O₃ (sapphire) as an example of substantial surface modification. The slightly defocused BF-TEM image of the substrate, Figure 5b, shows the nanometer-sized “pits” in sapphire after

FIB preparation at 5 keV, which are eliminated by the sequential milling of the specimen at 900 and 500 eV with a concentrated Ar ion beam, as shown in Figures 5c and 5d.

The vertical contrast lines visible in Figures 5a, and 5b are due to the so-called “curtaining effect” (Giannuzzi & Stevie, 1999), which forms due to sputtering rate differences in the specimen. The main source of curtaining in this specimen was the relatively rough polycrystalline structure of the ion beam-deposited Pt/C protective layer. The “curtaining” effect can be greatly reduced by depositing a homogenous protective layer on the top of the samples, for example, pure carbon or tungsten, in the FIB. In addition, the NanoMill system ion milling process minimizes the curtaining effect, as shown in Figures 5c and 5d.

Examples for Quantitative TEM (aberration corrected)

In addition to the possibility of reducing the surface damage layer, the adjustment of the layer thickness is equally important for quantitative studies of material properties using aberration-corrected TEM, which often requires fixed

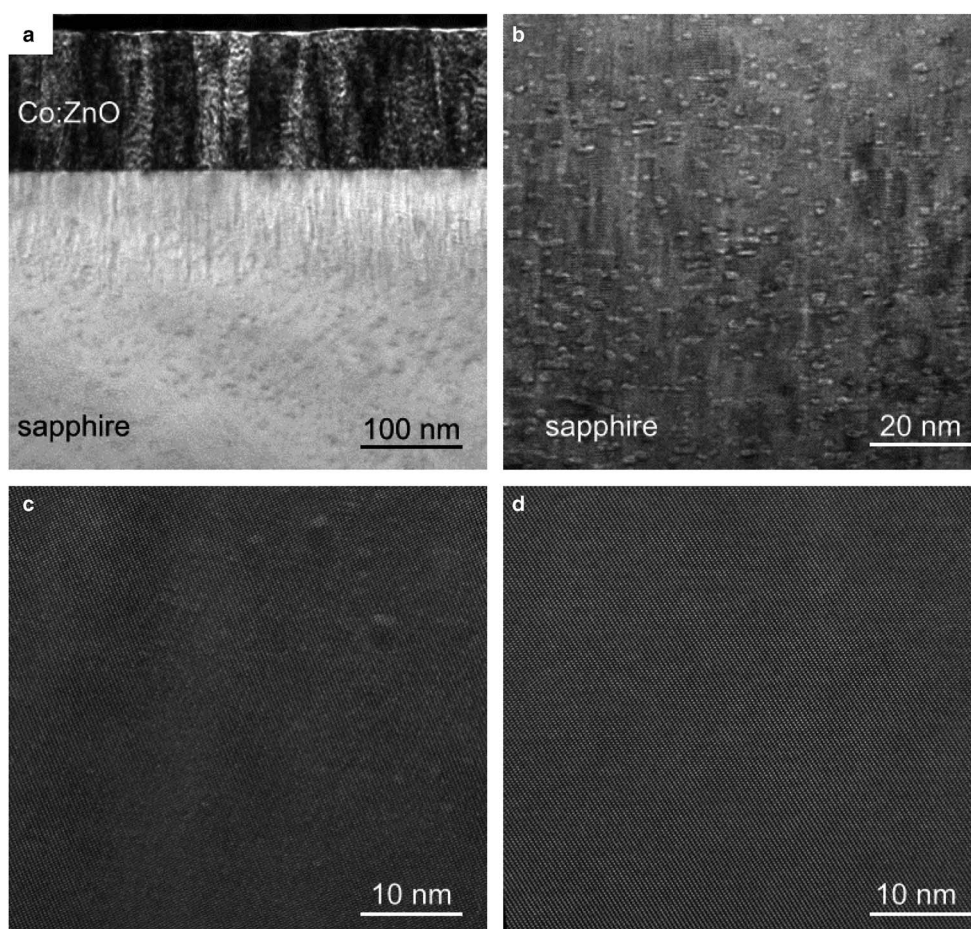


Figure 5. **a:** Bright-field transmission electron microscopy image of Co-doped ZnO thin film deposited on sapphire substrate after the focused ion beam preparation finished at 5 keV. The specimen thickness is ~100 nm. **b:** Magnified image of the sapphire substrate showing round shape contrast of hollow regions and line contrast of a curtaining effect. **c:** High-resolution transmission electron microscopy (HRTEM) image of sapphire after milling at 900 eV for 5 min with Ar ions. **d:** HRTEM image of sapphire after milling at 500 eV for an additional 15 min with Ar ions.

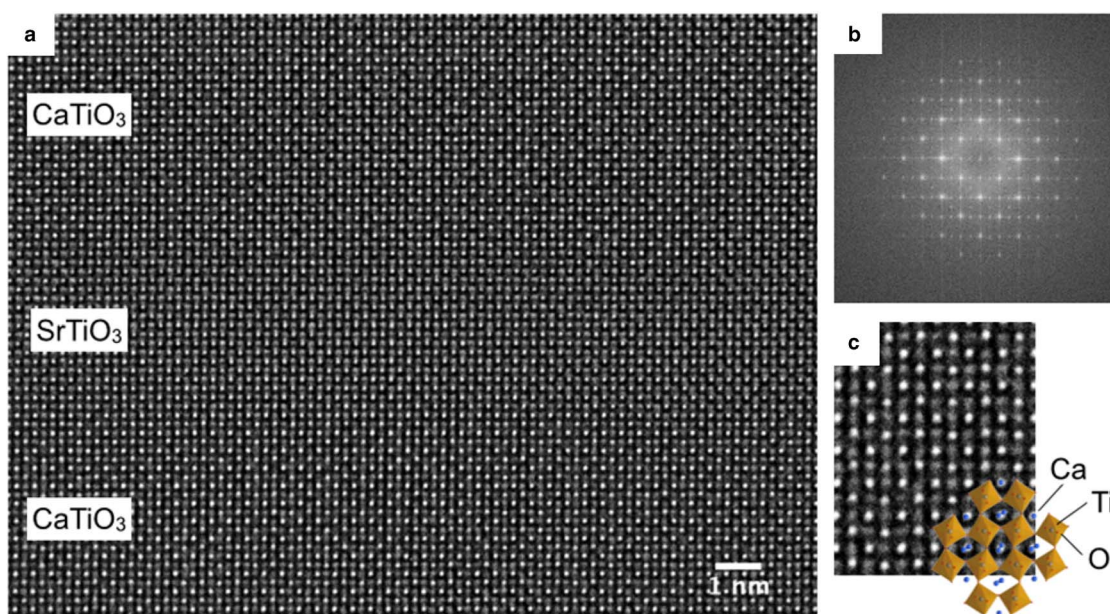


Figure 6. a: Unprocessed aberration-corrected high-resolution transmission electron microscopy image of CaTiO_3 and SrTiO_3 multilayer and its Fourier transform shown in (b). c: Part of the CaTiO_3 layer displayed in larger magnification together with a schematic of the atomic structure. Clearly, oxygen columns are resolved.

and/or very thin specimen thickness—in some cases, <10 nm (Jia et al., 2010). Specimen thickness is also an important factor in studies of beam-sensitive materials because they require low-acceleration voltages (<100 keV) in the TEM.

Figure 6 shows a HRTEM image of a $\text{CaTiO}_3/\text{SrTiO}_3$ multilayer specimen recorded at negative C_s conditions (Jia et al., 2010) using the spherical and chromatic aberration-corrected microscope operated at 80 keV. The FIB lamellae preparation was done in accordance with the steps shown in Table 1, whereas the final milling was done at 500 eV using Ar ions. Despite the low acceleration voltage, the atomic columns of Sr, Ti, and Ca are clearly resolved and relatively equal in brightness. In between these positions, weaker contrast produced by the oxygen columns are observed and shown in Figure 6c.

Although the HRTEM image represents the pinnacle of quantitative TEM imaging due to specimen and instrumentation; of equal importance is the more commonly applied technique of quantitative HAADF-STEM imaging (LeBeau et al., 2008; LeBeau et al., 2009; LeBeau et al., 2010a, 2010b). This technique requires linearization of the HAADF detector, which has shown that column intensity scales with atomic number (Z) $\sim Z^{1.6-1.9}$ (Hartel et al., 1996; Rafferty et al., 2001) through incoherent signal collection. For clean specimens <10 nm in thickness, it is possible to chemically identify atomic columns determined by the corresponding HAADF intensity. A specimen that permits quantitative HAADF-STEM imaging and the corresponding column identification is shown in Figures 7a and 7b, respectively (Hauser et al., 2011). The HAADF image was acquired using a third-order aberration- and probe-corrected Titan STEM equipped with an annular dark-field

detector (E.A. Fischione Instruments, Inc.). The STEM was operated at 300 keV and is presented with no image filtering to highlight the uniform imaging conditions possible following low-energy Ar ion milling, which reduces residual surface artifacts.

Examples of Structural Metallurgical Alloys

A common technique for the analysis of metallurgical specimens is the preparation of 3 mm discs by mechanical dimpling and broad-beam ion milling. The final surface quality of 3 mm discs and the corresponding analytical electron microscopy results can be improved with low-energy Ar ion milling. This approach is also useful for specimens that acquire surface oxidation during storage.

Results obtained for a Ni-based superalloy specimen that was dimpled mechanically and broad-beam milled (5 keV with Ar ions) are shown in Figure 8a. The progressive improvement in HRTEM image clarity and the reduction of surface mottling related to the smoothing of topography as the incident Ar ion beam energy is reduced from 5 to 500 eV is observed in Figures 8b and 8c.

FIB preparation with a Ga ion beam for site specific, as well as crystallographically oriented, metallurgical specimens has become the preferred method for many researchers involved in characterizing deformation behavior along specific crystallographic planes. One of the most important aspects of structural alloy characterization when using the TEM is dislocation and defect analysis for correlation of the alloy's structure with mechanical behavior. Classically, this characterization was performed using diffraction contrast techniques and tilting to reveal the nature of the defects.

Table 1. Transmission Electron Microscopy (TEM) Specimen Preparation Steps and Main Parameters Using Focused Ion Beam (FIB) and the NanoMill TEM Specimen Preparation System.

	Specimen Preparation ^c	Beam Energy (keV)	Beam Current	Incident Angle	Size or Time	Remarks/Notes	
FIB Milling ^a	Pt/C protective layer deposition	5	55 pA	0°		<ul style="list-style-type: none"> • Electron beam used for deposition • Use is material dependent 	
	C protective layer deposition	5	55 pA	0°		<ul style="list-style-type: none"> • Electron beam used for deposition • Use is material dependent 	
	Pt/C protective layer deposition	30	0.28 nA	52°		Ga ion beam used	
	Trench cut	30	21 nA	52°	Two trenches, each 20 × 8 μm	Lamellae thickness down to ~ 3 μm	
	J-undercut	30	6.5 nA	7°			
	Lift out and weld the lamella to an Omniprobe grid using a micromanipulator					22.5 × 1 × 1.5 μm Pt strip at 30 keV, 48 pA	
	Thinning		30	2.8 nA	± 2°		Down to ~ 1.5 μm (CCS ^e)
			30	0.92 nA	± 1.5°		< 1 μm (CCS ^e)
			30	0.46 nA	± 1.5°		< 0.5 μm (CCS ^e)
			30	93 pA	± 1.2°		~ 0.2 μm (rectangular box)
	Thinning	5	47 pA	± 5°		~ 0.1 μm (rectangular box)	
NanoMilling process ^b	Thinning ^c	0.9	120 μA ^d	± 10°	~ 30 min	<ul style="list-style-type: none"> • Current is measured using a Faraday cup • Time is specimen dependent 	
	Thinning ^c	0.5	120 μA ^d	+ 12/-10°	~ 40 min	<ul style="list-style-type: none"> • Current is measured using a Faraday cup • Time is specimen dependent 	
	Thinning ^c	< 0.5	120 μA ^d	+ 14/-10°	~ 40 min	Beam-sensitive materials	
	Optional thinning at cryogenic temperature	0.2-0.9	120 μA ^d			<ul style="list-style-type: none"> • Beam-sensitive materials • Materials containing polymers 	

^aSteps may vary according to specimen material and requirements. Depositing a 20-nm thick Pt or C layer to the surface can reduce charging of insulating materials in the scanning electron microscope/FIB. FIB procedure is 2–4 h.

^bNanoMill system thinning ranges from a few minutes to 1 h and is largely dependent upon the initial lamella condition and, in particular, its corresponding thickness.

^cMilling time and incident angles depend on the material, damaged layer thickness, and required final thickness of the lamellae. Milling current is adjustable.

^dEmission current.

^eCCS, cleaning cross-section.

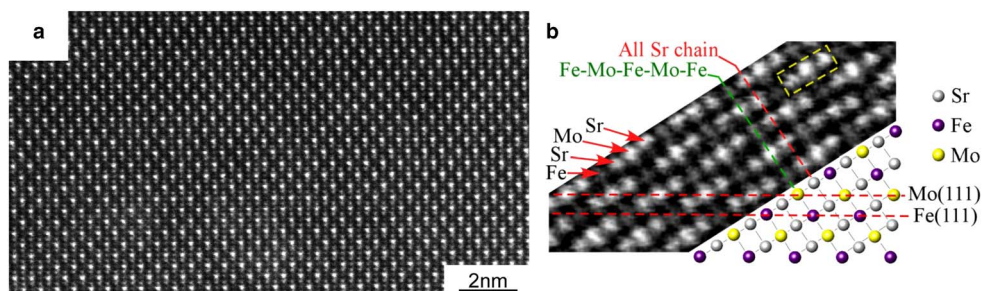


Figure 7. Unfiltered, aberration-corrected high-angle annular dark-field scanning transmission electron microscopy (HAADF-STEM) images of a $\text{Sr}_2\text{FeMoO}_6$ thin film grown on SrTiO_3 . **a:** Uniform, damage-minimized surface condition is shown. **b:** A schematic with the corresponding HAADF-STEM image showing the projection of the double perovskite ordering along the $\langle 110 \rangle$ and the Mo-Fe ordering separated by a Sr chain (Hauser et al., 2011).

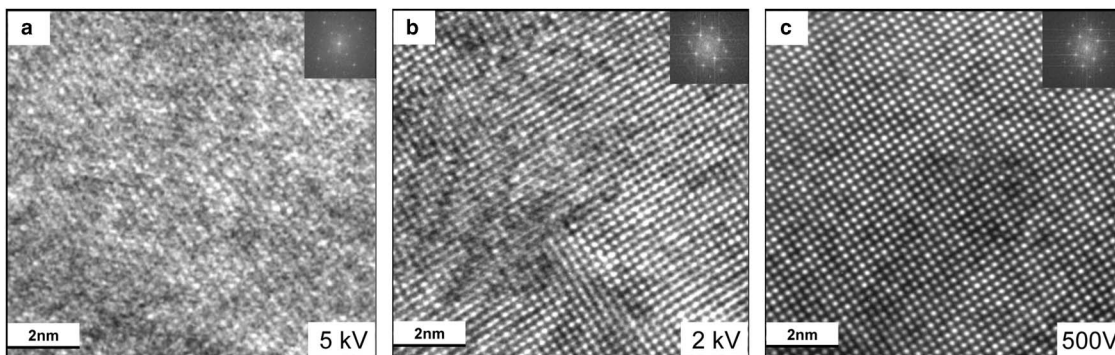


Figure 8. Improvement in high-resolution transmission electron microscopy images from a Ni-based superalloy specimen after successive applications of low-energy Ar ion milling are shown for the image quality following (a) broad-beam milling at 5 keV, (b) Ar ion milling at 2 keV and (c) 500 eV. The improvement in image quality is characterized with the inset fast Fourier transform for each image.

While diffraction contrast has been and will continue to be a vital characterization method for structural alloys using the TEM, one disadvantage associated with the diffraction contrast technique for defect analysis involves the very basis of the technique, namely dynamical scattering. For example, when characterizing dislocation substructures, the presence of bend contours and surface damage can obscure large parts of an image, as shown in Figure 9a.

Mills and his colleagues have shown that significant advantages may be accrued by using STEM to reduce the extent of the dynamical contrast, while retaining the ability to characterize defects following the traditional “TEM rules” of diffraction contrast (Phillips et al., 2011). This STEM technique allows a rapid characterization of dislocation substructures and permits the analysis of much thicker specimens, which enables the collection of more robust data. Figure 9b shows an increased magnification relative to Figure 9a, the oval indicates the same lath in both images. The dominant dark contrast, observed in Figure 9a, is indicative of the residual damage and amorphization that occurs during Ga ion milling. This diffraction contrast is prohibitive to analysis and must be removed for characterization of the salient microstructural features present in the alloy. The result of subsequent low-energy Ar ion milling of the surface

at 500 eV is shown in Figure 9b and reveals the dislocation substructure desired for analysis.

Not unexpectedly, the residual surface modifications from Ga ion milling also manifest in STEM diffraction contrast techniques and can prohibit characterization, as shown in Figure 10a. Figures 10a and 10c are bright-field STEM images of a structural titanium alloy. The subsequent improvement in imaging quality with decreasing ion milling beam energy is evident in Figure 10c—clear separation of dislocations and no undesirable contrast modulations in the matrix.

Specimen preparation artifacts can be resolution limiting for analytical TEM, in part due to surface modification and/or damage of the lattice, which results in scattering of the electron beam in an undesirable fashion and obscures microstructural features. FIB preparation is increasingly ubiquitous; thus, to prepare high-quality TEM specimens for qualitative and quantitative methods as shown above, low-kilovolt Ar ion milling is critical. The modified specimen surface layer may exhibit an altered chemical composition at interfaces of interest as a result of Ga FIB preparation. Our results show that uniform and damage-free specimens can be produced using the NanoMill system; a small spot from sufficiently low ion energy (as low as 50 eV) produces enough current (~ 100 – 150 pA) to allow for reasonable milling rates (~ 1 – 8 nm/min).

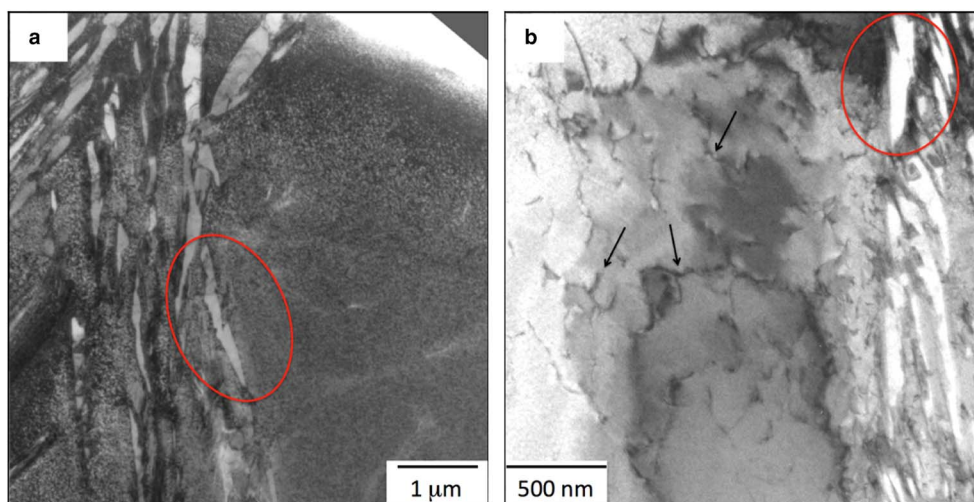


Figure 9. Conventional diffraction contrast images of a structural titanium alloy taken at different magnifications and areas showing the lath feature labeled in (a) and (b). The arrows in (b) indicate the dark linear features as dislocations. Note the marked reduction in “black spot” contrast when compared with (a), which permits clear observation of dislocations in (b) after NanoMilling.

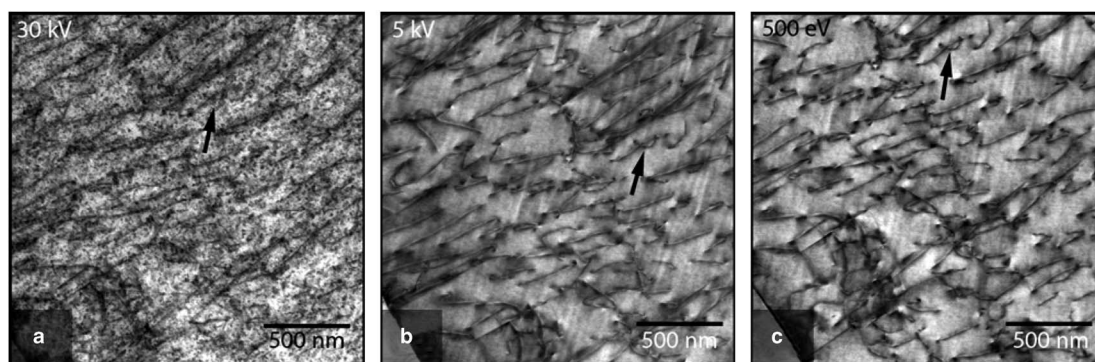


Figure 10. Bright-field scanning transmission electron microscopy images of a structural titanium alloy characterizing the dislocation structure. The arrows indicate the same dislocation in (a), (b), and (c). The black spots in (a) are indicative of diffraction contrast from 30 keV Ga ion surface modification and obscure the desired dislocation information. Although the image improved after 5 keV ion milling, the separation between dislocations is not as evident as observed in (c). The intensity variation between matrix and dislocation is maximized after 500 eV milling, (c).

CONCLUSIONS

State-of-the-art transmission electron microscopy often requires thin (<10 nm) specimens where possible amorphous surface layers are, at most, 0.5 nm. To match these criteria, FIB-prepared lamellae, for example, require post treatment by Ar ion milling to eliminate spurious results. In this work, an $\sim 1\ \mu\text{m}$ FWHM diameter, low-energy, concentrated, Ar ion beam successfully reduced the thickness of ion-damaged surface layers and prevented redeposition of sputtered material. Experiments revealed significant improvement in image quality for various materials of technological and scientific interest, which enabled the collection of accurate, quantitative metrics using a variety of analytical electron microscopy techniques, ranging from diffraction contrast to quantitative STEM imaging.

ACKNOWLEDGMENTS

The authors thank D. Meertens (Forschungszentrum Jülich, PGI-5) for the preparation of FIB lamellas. The MnAs and ZnO specimens were kindly provided by A. Ney (J. Kepler University, Linz, Austria). Appreciation is also extended to Joachim Mayer and Christian Kieselowski for their efforts in preparing and conducting the microscopy for the Si specimen.

REFERENCES

- ANDERSON, R. & KLEPEIS, S.J. (2005). Practical aspects of FIB TEM specimen preparation. In *Introduction to Focused Ion Beams: Instrumentation, Theory, Techniques, and Practice*, Giannuzzi, L.A. & Stevie, F.A. (Eds.), pp. 173–200. New York, NY: Springer.

- BAHNCK, D. & HULL, R. (1990). Experimental measurement of transmission electron microscope specimen temperature during ion milling. *MRS Online Proc Libr* **199**, 253.
- BARBER, D.J. (1993). Radiation damage in ion-milled specimens: Characteristics, effects and methods of damage limitation. *Ultramicroscopy* **52**(1), 101–125.
- BARNA, Á. (1991). Topographic kinetics and practice of low angle ion beam thinning. *MRS Online Proc Libr* **254**, 3–22.
- BARNA, Á., PÉCZ, B. & MENYHARD, M. (1998). Amorphisation and surface morphology development at low-energy ion milling. *Ultramicroscopy* **70**(3), 161–171.
- BARNA, Á., PÉCZ, B. & MENYHARD, M. (1999). TEM sample preparation by ion milling/amorphization. *Micron* **30**(3), 267–276.
- BARNARD, A.W., HYUN, J.K., GRAZUL, J.L. & MULLER, D.A. (2006). Surface roughness instabilities in low-angle ion milling. *Microsc Microanal* **12**(S02), 1318–1319.
- BASILE, D.P., BOYLAN, R., BAKER, B., HAYES, K. & SOZA, D. (1991). Fibxtm—Focussed ion beam milling for TEM sample preparation. *MRS Online Proc Libr* **254**, 23–41.
- BATSON, P.E., DELLBY, N. & KRIVANEK, O.L. (2002). Sub-Ångström resolution using aberration corrected electron optics. *Nature* **418**(6898), 617–620.
- COOPER, D., TRUCHE, R., TWITCHETT-HARRISON, A., DUNIN-BORKOWSKI, R.E. & MIDGLEY, P. (2009). Quantitative off-axis electron holography of GaAs p-n junctions prepared by focused ion beam milling. *J Microsc* **233**(1), 102–113.
- DAS, A.K., PAMPUCH, C., NEY, A., HESJEDAL, T., DÄWERITZ, L., KOCH, R. & PLOOG, K.H. (2003). Ferromagnetism of MnAs studied by heteroepitaxial films on GaAs(001). *Phys Rev Lett* **91**(8), 087203.
- GENÇ, A., OHIO STATE UNIVERSITY & E.A. FISCHIONE INSTRUMENTS INC (2007). Post-FIB TEM sample preparation using a low energy argon beam. *Microsc Microanal* **13**(S02), 1520–1521.
- GIANNUZZI, L.A. (2006). Reducing FIB damage using low energy ions. *Microsc Microanal* **12**(S02), 1260–1261.
- GIANNUZZI, L.A. & STEVIE, F.A. (1999). A review of focused ion beam milling techniques for TEM specimen preparation. *Micron* **30**(3), 197–204.
- HARTEL, P., ROSE, H. & DINGES, C. (1996). Conditions and reasons for incoherent imaging in STEM. *Ultramicroscopy* **63**(2), 93–114.
- HAUSER, A.J., WILLIAMS, R.E., RICCIARDO, R.A., GENÇ, A., DIXIT, M., LUCY, J.M., WOODWARD, P.M., FRASER, H.L. & YANG, F. (2011). Unlocking the potential of half-metallic Sr₂FeMoO₆ films through controlled stoichiometry and double-perovskite ordering. *Phys Rev B* **83**(1), 014407.
- HUH, Y., HONG, K. & SHIN, K. (2013). Amorphization induced by focused ion beam milling in metallic and electronic materials. *Microsc Microanal* **19**(S5), 33–37.
- JIA, C.L., HOUBEN, L., THUST, A. & BARTHEL, J. (2010). On the benefit of the negative-spherical-aberration imaging technique for quantitative HRTEM. *Ultramicroscopy* **110**(5), 500–505.
- JIA, C.L., MI, S.B., BARTHEL, J., WANG, D.W., DUNIN-BORKOWSKI, R.E., URBAN, K.W. & THUST, A. (2014). Determination of the 3D shape of a nanoscale crystal with atomic resolution from a single image. *Nat Mater* **13**(11), 1044–1049.
- KAMINO, T., YAGUCHI, T., HASHIMOTO, T., OHNISHI, T. & UMEMURA, K. (2005). A FIB micro-sampling technique and a site specific TEM specimen preparation method. In *Introduction to Focused Ion Beams: Instrumentation, Theory, Techniques, and Practice*, Giannuzzi, L.A. & Stevie, F.A. (Eds.), pp. 229–245. New York, NY: Springer Science+Business Media, Inc.
- KATO, N.I. (2004). Reducing focused ion beam damage to transmission electron microscopy samples. *J Electron Microsc* **53**(5), 451–458.
- KIRK, E.C., WILLIAMS, D.A. & AHMED, H. (1989). Cross-sectional transmission electron microscopy of precisely selected regions from semiconductor devices. *Inst Phys Conf Ser* **100**, 501–506.
- KOVÁCS, A., NEY, A., DUCHAMP, M., NEY, V., BOOTHROYD, C.B., GALINDO, P.L., KASPAR, T.C., CHAMBERS, S.A. & DUNIN-BORKOWSKI, R.E. (2013). Defects in paramagnetic Co-doped ZnO films studied by transmission electron microscopy. *J Appl Phys* **114**, 243503.
- LEBEAU, J.M., D'ALFONSO, A.J., FINDLAY, S.D., STEMMER, S. & ALLEN, L.J. (2009). Quantitative comparisons of contrast in experimental and simulated bright-field scanning transmission electron microscopy images. *Phys Rev B* **80**(17), 174106.
- LEBEAU, J.M., FINDLAY, S.D., ALLEN, L.J. & STEMMER, S. (2008). Quantitative atomic resolution scanning transmission electron microscopy. *Phys Rev Lett* **100**(20), 206101.
- LEBEAU, J.M., FINDLAY, S.D., ALLEN, L.J. & STEMMER, S. (2010a). Position averaged convergent beam electron diffraction: Theory and applications. *Ultramicroscopy* **110**(2), 118–125.
- LEBEAU, J.M., FINDLAY, S.D., ALLEN, L.J. & STEMMER, S. (2010b). Standardless atom counting in scanning transmission electron microscopy. *Nano Lett* **10**(11), 4405–4408.
- LI, L. & YANG, J.C. (2002). Oxide structures formed on silver single crystals due to hyperthermal atomic oxygen exposure. *MRS Online Proc Libr* **751**, Z3.37.
- LOTNYK, A., POPPITZ, D., ROSS, U., GERLACH, J., FROST, F., BERNÜTZ, S., THELANDER, E. & RAUSCHENBACH, B. (2015). Focused high- and low-energy ion milling for TEM specimen preparation. *Microelectron Reliab* **55**(9–10), 2119–2125.
- MAYER, J., GIANNUZZI, L.A., KAMINO, T. & MICHAEL, J. (2007). TEM sample preparation and FIB-induced damage. *MRS Bull* **32**(5), 400–407.
- MCCAFFREY, J.P., PHANEUF, M.W. & MADSEN, L.D. (2001). Surface damage formation during ion-beam thinning of samples for transmission electron microscopy. *Ultramicroscopy* **87**, 97–104.
- MEHRTENS, T., BLEY, S., VENKATA SATYAM, P. & ROSENAUER, A. (2012). Optimization of the preparation of GaN-based specimens with low-energy ion milling for (S)TEM. *Micron* **43**(8), 902–909.
- MIJAJIMA, N., HOLZAPFEL, C., ASAHARA, Y., DUBROVINSKY, L., FROST, D., RUBIE, D., DRECHSLER, M., NIWA, K., ICHIHARA, M. & YAGI, T. (2010). Combining FIB milling and conventional Argon ion milling techniques to prepare high-quality site-specific TEM samples for quantitative EELS analysis of oxygen in molten iron. *J Microsc* **238**(3), 200–209.
- MKHOYAN, K., BABINEC, T., MACCAGNANO, S., KIRKLAND, E. & SILCOX, J. (2007). Separation of bulk and surface-losses in low-loss EELS measurements in STEM. *Ultramicroscopy* **107**(4–5), 345–355.
- MOBERLYCHAN, W.J., ADAMS, D.P., AZIZ, M.J., HOBLER, G. & SCHENKEL, T. (2007). Fundamentals of focused ion beam nanostructural processing: Below, at, and above the surface. *MRS Bull* **32**(5), 424–432.
- PHILLIPS, P.J., BRANDES, M.C., MILLS, M.J. & DE GRAEF, M. (2011). Diffraction contrast STEM of dislocations: Imaging and simulations. *Ultramicroscopy* **111**(9–10), 1483–1487.
- RAFFERTY, B., NELLIST, D. & PENNYCOOK, J. (2001). On the origin of transverse incoherence in Z-contrast STEM. *J Electron Microsc* **50**(3), 227–233.
- SCHAFFER, M., SCHAFER, B. & RAMASSE, Q. (2012). Sample preparation for atomic-resolution STEM at low voltages by FIB. *Ultramicroscopy* **114**, 62–71.

- SCHEU, C., GAO, M., VAN BENTHEM, K., TSUKIMOTO, S., SCHMIDT, S., SIGLE, W., RICHTER, G. & THOMAS, J. (2003). Advances in EELS spectroscopy by using new detector and new specimen preparation technologies. *J Microsc* **210**(1), 16–24.
- UNOCIC, K.A., MILLS, M.J. & DAEHN, G.S. (2010). Effect of gallium focused ion beam milling on preparation of aluminium thin foils. *J Microsc* **240**(3), 227–238.
- UTKE, I., HOFFMANN, P. & MELNGAILIS, J. (2008). Gas-assisted focused electron beam and ion beam processing and fabrication. *J Vac Sci Technol B* **26**(4), 1197–1276.
- VOLKERT, C.A. & MINOR, A.M. (2007). Focused ion beam microscopy and micromachining. *MRS Bull* **32**(5), 389–399.
- YOUNG, R.J., KIRK, E.C., WILLIAMS, D.A. & AHMED, H. (1990). Fabrication of planar and cross-sectional TEM specimens using a focused ion beam. *MRS Online Proc Libr* **199**, 205–216.